Topology optimization design of resonant

structures based on antiresonance

eigenfrequency matching informed by

4 harmonic analysis

5	
6	Giraldo Guzman, Daniel ¹
7	Pennsylvania State University
8	327 Leonhard Building, University Park, PA 16802
9	dzg5526@psu.edu
10	
11	Lissenden, Clifford
12	Pennsylvania State University
13	212 Earth and Engineering Sciences Building, University Park, PA 16802
14	cjl9@psu.edu
15	ASME Fellow
16	
17	Shokouhi, Parisa
18	Pennsylvania State University
19	411 Earth and Engineering Sciences Building, University Park, PA 16802
20	pxs990@psu.edu
21	
22	Frecker, Mary
23	Pennsylvania State University
24	136 Reber Building, University Park, PA 16802
25	mxf36@psu.edu
26	ASME Fellow

¹ Corresponding author

ABSTRACT

27

28

29

30

31

32

33

34

35

36

37

38

39

40

41

42

43

44

45

46

In this paper, we present a design methodology for resonant structures exhibiting particular dynamic responses by combining an eigenfrequency matching approach and a harmonic analysis-informed eigenmode identification strategy. This systematic design methodology, based on topology optimization, introduces a novel computationally efficient approach for 3D dynamic problems requiring antiresonances at specific target frequencies subject to specific harmonic loads. The optimization's objective function minimizes the error between target antiresonance frequencies and the actual structure's antiresonance eigenfrequencies, while the harmonic analysis-informed identification strategy compares harmonic displacement responses against eigenvectors using a modal assurance criterion, therefore ensuring an accurate recognition and selection of appropriate antiresonance eigenmodes used during the optimization process. At the same time, this method effectively prevents well-known problems in topology optimization of eigenfrequencies such as localized eigenmodes in low-density regions, eigenmodes switching order, and repeated eigenfrequencies. Additionally, our proposed localized eigenmode identification approach completely removes the spurious eigenmodes from the optimization problem by analyzing the eigenvectors' response in low-density regions compared to high-density regions. The topology optimization problem is formulated with a density-based parametrization and solved with a gradient-based sequential linear programming method, including material interpolation models and topological filters. Two case studies demonstrate that the proposed design methodology successfully generates antiresonances at the desired target frequency subject to different harmonic loads, design domain dimensions, mesh discretization, or material properties.

47

48

Keywords: Topology optimization, Eigenfrequency matching, Frequency response analysis, Antiresonances

1. INTRODUCTION

Devising effective means to control wave propagation is of paramount importance across length scales, from designing electronic devices to vibration isolation of critical structures. In search of effective means, an approach inspired by the concept of locally resonant metamaterials uses sub-wavelength resonators to create frequency bandgaps [1], i.e., a frequency range where waves do not propagate. A sub-class of these metamaterials composed of surface-mounted or surface-embedded resonators are called Locally Resonant Metasurfaces (LRM). These LRM are fundamentally different from phononic crystals whose working mechanisms, explained by Bragg scattering [2], depend upon the periodicity of their unit cells. Instead, LRM rely on interactions between the propagating wave and the local resonator's response, exhibiting scattering and non-conventional dispersion properties that lead to frequency bandgaps [3]. When these LRM are used to control elastic guided wave propagation, e.g. Lamb or Rayleigh waves, they are called Elastodynamic LRM (ELRM).

Since the introduction of ELRM, their local resonator designs have been based on simple geometries, i.e., rods, holes, spheres, beams, or simply mass-spring systems. These designs often rely on the parametric tuning of geometrical features empirically [4]–[9], or experimentally [10]–[14] until the desired bandgap is achieved. Optimization and machine learning methods have been used to tailor dispersion curves [15]–[21] or effective material properties [22]–[25] mainly for 2D phononic crystals assuming periodicity of unit cells, however, a rational design methodology to tailor the local

resonator's response to particular wave excitations is missing. Our investigation [26]–[28] demonstrates that the local resonator's *antiresonances* are the key factor in generating frequency bandgaps for ELRM. Thus, the motivation of our work is how to design resonant structures by tailoring their antiresonances. This paper establishes a generalized systematic design methodology to conceive resonant structures based on antiresonance matching. One of the methodology's applications is the design of local resonators for ELRM, however, it is applicable to any design problem requiring antiresonance manipulation.

The Topology Optimization (TO) method [29], which is of particular interest to this study, is a computational tool to design complex layouts in numerous applications [30]–[32] and it has been proven to be a robust design tool for dynamic problems [33], [34]. Previous works on TO have attempted to manipulate antiresonances with harmonic-based formulations such as the minimum dynamic compliance [35]–[37], solving mostly 2D problems with only a few design variables and surrogate formulations to reduce computational load. 3D problems have significantly more design variables, resulting in complex and expensive computational tasks [38]. Moreover, the dynamic compliance could be undefined around an antiresonance frequency [36], [39], making the minimum dynamic compliance problem not suitable for antiresonance manipulation. Thus, a harmonic-based TO is not feasible. Instead, we propose an approach that relies on manipulating eigenfrequencies which are significantly less expensive to compute, in

conjunction with a harmonic-informed selection of antiresonance eigenmodes to be used within the optimization process.

94

95

96

97

98

99

100

101

102

103

104

105

106

107

108

109

110

111

112

113

92

93

The eigenfrequency problem is well-known in TO. It has been commonly used from three different approaches [38]: maximize the structure's eigenfrequencies [40], generate a gap in-between eigenfrequencies [41], and match the structure's eigenfrequencies with target frequencies [42]. The last approach, which is most relevant to this paper, has been mostly used to match resonance eigenfrequencies without considering how dynamic forces interact with the structure, an important consideration for the antiresonance matching problem. This is because matching eigenfrequencies for resonances or antiresonances are fundamentally different problems. Resonances occur when a dynamic force excites the structure's natural frequencies of resonance, namely, resonance eigenfrequencies. On the other hand, antiresonances occur when the dynamic force is out of phase with respect to the structure's response, resulting in zero or near-to-zero displacement(s) at a particular location(s); the dynamic load cancels out with an equal but opposite reaction force, equivalent to constraining the displacement(s) at that point(s) [43]. The antiresonance frequencies of the dynamically-loaded structure correlate with specific eigenfrequencies of the displacement-constrained structure [44]. Here, we refer to those displacement-constrained eigenfrequencies as the antiresonance eigenfrequencies. Contrary to resonance eigenmodes, several antiresonance eigenmodes are not excited by particular dynamic loads, making the selection of these eigenmodes a critical component of the antiresonance eigenfrequency matching approach. Thus, the commonly used eigenfrequency matching approaches do not work for the antiresonance matching problem as it needs additional information to appropriately select antiresonance eigenmodes considering specific dynamic loads. This paper presents a new harmonic-informed eigenfrequency matching approach that properly identifies the particular antiresonance eigenmodes to be optimized.

This paper presents a twofold contribution: (i) a computationally feasible design methodology for 3D structures exhibiting antiresonances at desired target frequencies using a density-based TO combining eigenfrequency matching and harmonic analyses, and (ii) a new analysis procedure to identify specific antiresonance eigenmodes using a harmonic-informed identification scheme, effectively preventing several problems reported in the literature for the eigenfrequency optimization problem. The remainder of this paper is organized into three sections: Section 2 introduces the design methodology, Section 3 presents two case studies and their corresponding analysis, and Section 4 summarizes our findings and discusses future work.

2. DESIGN METHODOLOGY

This section presents a design methodology seeking to generalize a topology optimization problem in which a structure's dynamic response is tailored by manipulating antiresonance eigenfrequencies with a harmonic-informed selection of eigenmodes.

2.1. Optimization problem

The optimization problem seeks to match a structure's antiresonance eigenfrequency with a predefined target frequency. The structure is systematically modified until the desired antiresonance eigenfrequency is achieved as closely as possible. The objective function minimizes the error between a target frequency f_T and the structure's antiresonance eigenfrequency f_A selected by a harmonic-informed analysis routine. Thus, the optimization problem formulation is:

$$\min_{\rho} \left(\frac{f_A - f_T}{f_T} \right)^2 \tag{1}$$

141 subject to:

$$0 < \rho_{min} \le \rho_e \le 1$$

$$V_{min} \le \sum_{e=1}^{N_e} \rho_e V_e \le V_{max}$$

$$([K] - \lambda_A [M]) \{\Phi_A\} = 0$$

$$(2)$$

where ρ are the pseudo-densities, namely design variables. Equation (2) presents the optimization constraints, where ρ_e is the pseudo-density of element e, with N_e the total number of finite elements. The minimum pseudo-density, set to $\rho_{min}=1\times 10^{-6}$,

prevents numerical problems. $\rho_e V_e$ is the effective volume of element e, and the maximum and minimum volume constraints are, respectively, V_{max} and V_{min} . [K] and [M] are, respectively, the global stiffness and mass matrices, and Φ_A is the eigenvector corresponding to the eigenvalue $\lambda_A = (2\pi f_A)^2$.

2.2. Optimization solver

Different optimization methods can be used to solve a TO design problem, e.g., optimality criteria, moving asymptotes, sequential programming, evolutionary algorithms, or level-set methods [20, 21]. Among these methods, sequential programming uses efficient algorithms for nonlinear problems [46]. Specifically, Sequential Linear Programming (SLP) is a popular method in structural optimization to deal with the nonlinear nature of complex problems because of its simplicity and the possibility to use efficient linear solvers, e.g., Simplex [47]. The SLP method requires a first-order linearization of the optimization problem, which is then sequentially solved by setting move limits on the design variables, converging to a local minimum of the nonlinear problem. Specifically, for this design methodology, the move limits' lower and upper bounds have been set to $LB_j = \rho_j - 0.01$ and $UB_j = \rho_j + 0.01$. The objective function in Equation (1) is linearized using first-order Taylor series as:

$$\min_{\rho} \frac{\partial}{\partial \rho_k} \left[\left(\frac{f_A - f_T}{f_T} \right)^2 \right] \rho_k \tag{3}$$

163 The linearized objective function simplifies to:

$$\min_{\rho} \left[\frac{(f_A - f_T)}{4\pi^2 f_A f_T^2} \frac{\partial \lambda_A}{\partial \rho_k} \right] \rho_k \tag{4}$$

164 where:

$$\frac{\partial \lambda_A}{\partial \rho_k} = \frac{\Phi_A^T \left(\frac{\partial [K]}{\partial \rho_k} - \lambda_A \frac{\partial [M]}{\partial \rho_k}\right) \Phi_A}{\Phi_A^T [M] \Phi_A} \tag{5}$$

165

166

167

168

169

170

171

172

2.3. Harmonic-informed selection of eigenmodes

- Identifying appropriate antiresonance eigenfrequencies to be matched with the target frequency is critical to ensure feasible solutions. By analyzing the structure's Frequency Response Function (FRF) at each iteration, suitable antiresonances are identified. The eigenmodes corresponding to these antiresonances are selected as appropriate modes to use during the optimization process. The harmonic analysis-informed identification approach consists of the following steps:
- Compute antiresonance eigenvalues $\{\lambda\}$ and eigenvectors $[\Phi]$:
- 174 $[K][\Phi] = {\lambda}[M][\Phi]$
- Delete rigid body eigenmodes below a threshold of 1Hz
- Remove localized eigenmodes using the routine detailed in APPENDIX A.
- Compute the structure's harmonic response to the harmonic force $F_{\rm Harmonic}$
- 178 $[M]\{\ddot{x}\} + [C]\{\dot{x}\} + [K]\{x\} = \{F_{\text{Harmonic}}\}$
- Extract the averaged FRF at the points of interest:
- averaged_FRF = mean(FRF)
- Find local antiresonance peaks using the MATLAB function findpeaks:

- [Amplitude,idx,Width,Prominence] = findpeaks(1/averaged FRF)
- Evaluate local peak frequency distance to target frequency g_a :
- 184 Proximity = abs(Target Peak Frequency)
- Evaluate metrics for each local antiresonance peak identified, i.e., antiresonance bandwidth, amplitude, prominence, and proximity to the target frequency g_a .
- Define a combined antiresonance evaluation factor as:
- 188 factor = Amplitude + Prominence + Width Proximity
- Select the local antiresonance peak with the highest evaluation factor as the
- 190 identified antiresonance frequency A_f .
- Extract the harmonic displacement response x_H at the identified frequency A_f .
- Evaluate the Modal Assurance Criterion (MAC) [48] between the harmonic
- displacement response x_H and all the antiresonance eigenvectors Φ_A :

194
$$MAC = \frac{|\boldsymbol{\phi}_A^T \boldsymbol{x}_H|^2}{(\boldsymbol{\phi}_A^T \boldsymbol{\phi}_A)(\boldsymbol{\phi}_A^T \boldsymbol{x}_H)}$$

- Select the eigenmode with the highest MAC coefficient as the identified antiresonance eigenmode; its corresponding eigenvalue $\lambda_A = (2\pi f_A)^2$ is used
- during the optimization in Equation (1).
- 198 The reader is referred to APPENDIX A. for a step-by-step explanation.

199

200

2.4. Topology optimization parametrization

- 201 A density-based TO problem is ideally a binary problem, having the design variables either
- 202 0 or 1 representing void or solid material, however, this is an ill-posed optimization
- 203 problem. Relaxing the solution space is necessary to allow for intermediate values in-

between 0 and 1, mathematically introducing artificial material properties; this is done by introducing material interpolation models [49]. Two models widely used in TO are the Solid Isotropic Material with Penalization (SIMP) model [50]:

$$E_e = \rho_e^p E_0 \tag{6}$$

and the Rational Approximation of Material Properties (RAMP) model [51]:

$$E_e = \frac{\rho_e}{1 + p(1 - \rho_e)} E_0 \tag{7}$$

where E_e is the interpolated material property for element e, E_0 is the original material property, and p is the penalization factor. Note that E may represent stiffness, mass, or damping. Typical penalization factors for stiffness (p_K) and mass (p_M) are, respectively, $p_K=3$ and $p_M=1$ [40], [52]–[55]. However, this combination of penalization factors promotes the generation of spurious localized eigenmodes in low-pseudo-density regions as it is shown in APPENDIX B. Thus, this design methodology uses the same penalization factors, i.e. $p_K=p_M$, regardless of the interpolation model.

2.5. Topology optimization problems in eigenfrequency approaches

In density-based TO, it is necessary to address problems such as checkerboard solutions, mesh dependency, or non-feasible solutions [31]. Moreover, the eigenfrequency matching approach presents other problems such as eigenmodes switching order or repeated eigenfrequencies [42], localized eigenmodes in low-density regions [40], and disconnected members [56]. The following solutions are proposed in this design methodology.

Eigenmode switching order or repeated eigenfrequencies. Ma et al [42] introduced the mean-eigenvalue formulation to overcome these problems, although it only works for multiple eigenfrequencies. Kim [57] introduced a tracking mode scheme that allows the tracking of single eigenmodes, although the tracked eigenmodes must be prescribed in advance. In this design methodology, these problems are overcome by matching eigenvectors with a harmonic response at an antiresonance frequency, as it is explained in Section 2.3 and detailed in APPENDIX A.

Localized eigenmodes. This problem was originally addressed by Neves et al. [58] by removing the low-density elements from the stiffness matrix; this approach modifies the design domain at each iteration, which is not feasible in density-based TO. Several approaches appear in the literature. Pedersen [40] modified the penalization stiffness-to-mass ratio (p_K/p_M) in low-density regions. Tcherniak [53], and Du and Olhoff [52] set the mass matrix penalization to zero or near-to-zero in low-density regions, therefore modifying the stiffness-to-mass ratio. Similarly, Zhang et al. [55], Rong [59], and Zhang [60] used different penalization schemes for the stiffness and mass matrices combining SIMP and RAMP interpolation models. All these papers have reported improvements in the localized eigenmodes problem by modifying the stiffness-to-mass ratio, mostly for the maximizing eigenfrequencies problem [40], however, for the antiresonance matching problem we have not seen the same results, as explained in APPENDIX B. This design methodology considers a constant ratio $p_K/p_M = 1$, i.e., all interpolation models and penalization factors are applied equally for stiffness, mass, and damping. On another note,

Li et al. [56] pointed out another kind of localized eigenmodes, not for low-density elements but for disconnected floating members. Li et al. proposed a recognition technique to remove these localized eigenmodes for a level-set TO. Here we propose a new localized eigenmode recognition and elimination routine for density-based TO that removes both the low-density and the disconnected members localized eigenmodes, as mentioned in Section 2.3 and detailed in APPENDIX A.

Disconnected members. Detached or isolated structural members are usually considered a problem in TO, especially for static problems such as the minimum compliance optimization. This problem is commonly solved by making these members inefficient by using volume constraints, interpolations models, and topological filters. However, in dynamic problems such as the antiresonance matching optimization, disconnected members do not help nor restrain the optimization from achieving the design objective, provided they are fully disconnected from the main body, i.e., without soft connections. APPENDIX C. shows that volume constraints failed to prevent disconnected members and demonstrates that disconnected members do not influence the dynamic response either. Nonetheless, this design methodology uses a filtering scheme to reduce softly-connected members proposed by Xu et al. [61] known as the "Projection filter", combining a density filter, Equation (8), and a Heaviside filter, Equation (9).

$$\bar{\rho}_e = \frac{\sum_{i \in N_s} w_i v_i \rho_i}{\sum_{i \in N_s} w_i v_i} \tag{8}$$

where N_s is the set of elements within a filter radius R_f , such that $N_s = \{i \mid R_{ie} \leq R_f\}$ with $R_{ie} = \|c_i - c_e\|$ being the distance between the element centers e and i. The weights are $w_i = R_f - R_{ie}$. v_i and ρ_i are the volume and pseudo-density of element i, respectively.

$$\tilde{\rho}_{e} = \begin{cases} \eta \left[e^{-\beta \left(1 - \frac{\bar{\rho}_{e}}{\eta} \right)} - \left(1 - \frac{\bar{\rho}_{e}}{\eta} \right) e^{-\beta} \right] & 0 \leq \bar{\rho}_{e} \leq \eta \\ (1 - \eta) \left[1 - e^{-\beta \frac{(\bar{\rho}_{e} - \eta)}{(1 - \eta)}} + \frac{(\bar{\rho}_{e} - \eta) e^{-\beta}}{(1 - \eta)} \right] + \eta & \eta < \bar{\rho}_{e} \leq 1 \end{cases}$$

$$(9)$$

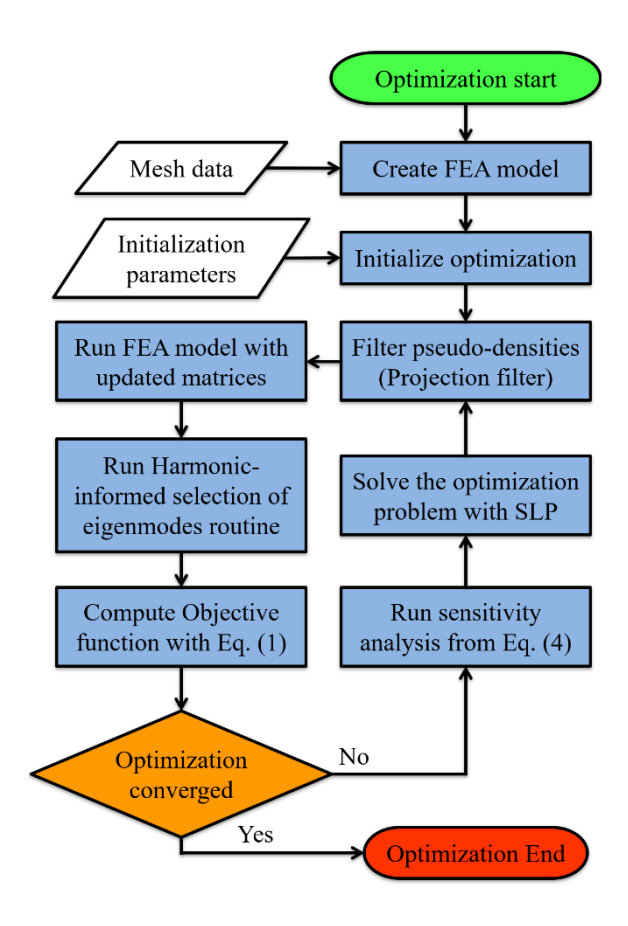
where $\bar{\rho}_e$ is the pseudo-density after density filtering and β controls the strength of the filter. In this design methodology, a continuation scheme is used, progressively increasing β to remove intermediate-density material, therefore promoting structural definition. The η parameter controls the volume during filtering. We preserve the volume after filtering by optimizing the η value with a bisection method at each iteration.

2.6. Optimization program

An optimization program to design resonating structures based on the proposed design methodology is implemented. This program, composed of multiple modules, integrates the software MATLAB and ABAQUS through PYTHON communication scripts [62], as shown in the flowchart of Figure 1. The optimization program starts with a finite element model data generation, including stiffness, mass, and damping matrices, mesh data with its nodal coordinates, element connectivity, loads, and boundary conditions. After this initialization, the optimization loop starts from the filters, followed by the Finite Element Analysis (FEA) considering matrices modified by filters and material interpolation models. The harmonic-informed routine from Section 2.3 analyses the topology's frequency

response at each iteration to select the most suitable eigenmode for computing the objective function (Equation (1)) and sensitivities (Equation (4)).

The proposed optimization workflow has been generalized to design any kind of structure by matching resonance or antiresonance eigenfrequencies. It can accommodate different material interpolation models, maximum and minimum volume constraints, solid or void non-design domains, numerical or analytical sensitivities, and multiple filtering schemes such as density, Heaviside, sensitivity, or move limits filters. Moreover, the integration with a commercial FEA software allows analysis of structures with complex geometries, multi-physics problems, and a variety of boundary conditions.



 ${\it Figure~1-Optimization~algorithm~flowchart}.$

3. CASE STUDIES

 This section illustrates the design of resonant structures using the methodology proposed in Section 2. Two case studies present resonator designs for different harmonic loads, frequency ranges, design domain dimensions, mesh discretization, and material properties. Figure 2 shows design domains with their mesh discretization for both case studies. Note that a symmetry condition on the xz-plane is used to reduce computation time. Table 1 lists the initial parameters for both case studies.

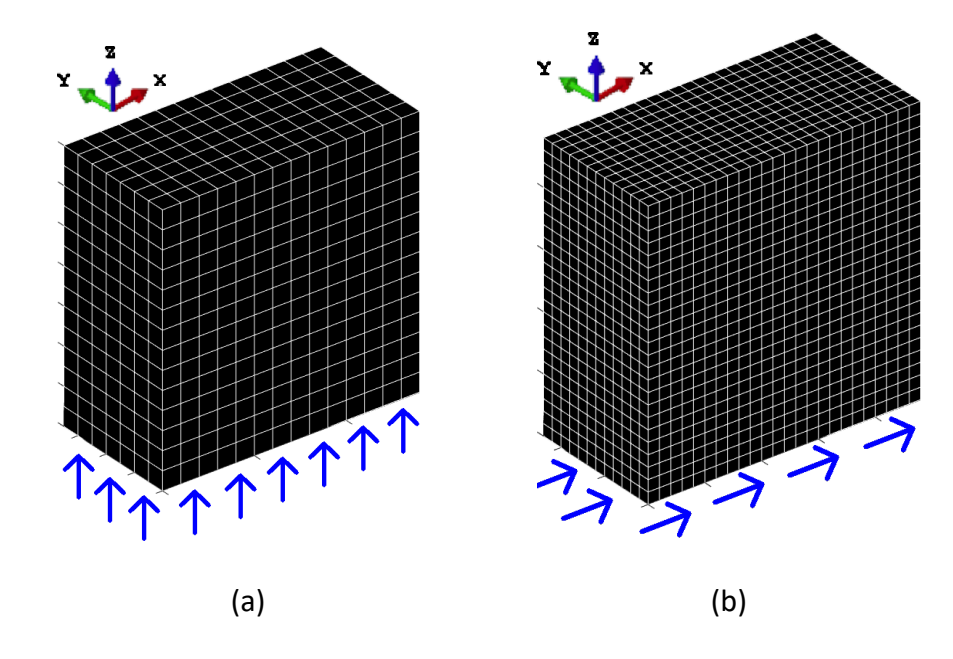


Figure 2 - Design domains with symmetry conditions on the xz-plane. Blue arrows show the direction of harmonic loads for each case study. Each voxel is a 20-node hexahedral finite element. (a) Case study #1: design domain of size 14x7x14 mm discretized with 1372 finite elements. (b) Case study #2: design domain of size 24x12x24 mm discretized with 6912 finite elements.

Table 1 - Initial parameters

Material properties, case study #1	E = 3.2516 GPa
	$\rho = 1222.2 \text{ kg/m}^3$
	v = 0.33
Material properties, case study #2	E = 69 [GPa]

$$\rho = 2730 \, [\text{kg/m}^3]$$

$$v = 0.33$$

Target antiresonance frequency f_T 30 kHz (case study #1)

50 kHz (case study #2)

Starting point ho Homogenous pseudo-density at $ho_e=0.5$

Solid non-design 4×2 [mm] bottom base

Void non-design all other first-layer elements

Maximum allowed volume $V_{max} = 90\%$

Minimum allowed volume $V_{min} = 10\%$

Interpolation model SIMP model

Penalization factors $p_K = p_M = 1$

Density filter radius R_f 3 [mm]

Heaviside filter β starting value $\beta = 20$

 β continuation scheme $\beta = \beta + 1$; at every iteration

311

312

313

314

315

316

317

318

319

320

321

The starting point considers all design variables to have the same pseudo-density, except for the bottom layer of elements, which considers a fully solid non-design bottom base at which the harmonic load must be applied, surrounded by void non-design elements. This is done to prevent numerical errors in the frequency response when harmonic loads are applied to void or near-to-void elements. The volume constraints are in place solely to prevent numerical instabilities in extreme cases, i.e., uncontrolled allocation of solid material or uncontrolled removal of material. However, the volume constraints do not play a major role in the proposed design methodology, as is usually done in topology optimization for lightweight structures. For a comparative study on how different volume constraints influence the solution, refer to APPENDIX C.

3.1. Case Study #1.

This case seeks to design a resonator that exhibits an antiresonance at 30 kHz subject to normal (out-of-plane) harmonic loads, as shown in Figure 2(a). Figure 3 shows the convergence history, Figure 4 shows the resultant optimized topology, and Figure 5 shows the topology's frequency response.

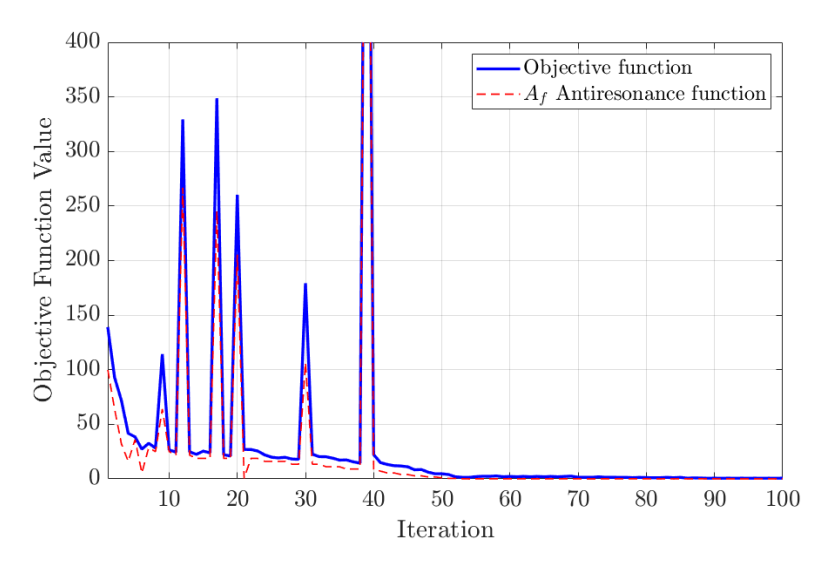


Figure 3 – Convergence history for 100 iterations (solid blue line), and antiresonance function (dashed red line) using $A_{\rm f}$ from the harmonic-informed routine of Section 2.3.

Figure 3 shows the objective function converging after iteration 52 with a value of 0.63. Several spikes are seen in the objective function before convergence. This phenomenon occurs when the harmonic-informed routine identifies an antiresonance with a high evaluation factor but low proximity to the target frequency, as described in Section 2.3; therefore, the objective function increases rapidly. The selection of an antiresonance closer to the target frequency is quickly recovered in the following iteration. This behavior is considered normal because the optimization explores the solution space for optimal solutions, especially during the first iterations, jumping to other potential solutions and

returning to the lowest value. Once the objective function has converged, the recognition of antiresonances is stable around the target frequency.

An antiresonance function has been computed by replacing the eigenfrequency f_g in Equation (1) with the antiresonance A_f identified by the harmonic-informed routine of Section 2.3. The correlation between the objective function and the antiresonance function in Figure 3 reveals whether the selected eigenfrequency accurately represents an antiresonance when the topology is subject to a specific harmonic loading condition. Figure 3 shows good agreement between the objective function and the antiresonance function, therefore validating our design methodology to tailor antiresonances using eigenfrequency matching with a harmonic-informed selection of eigenmodes.

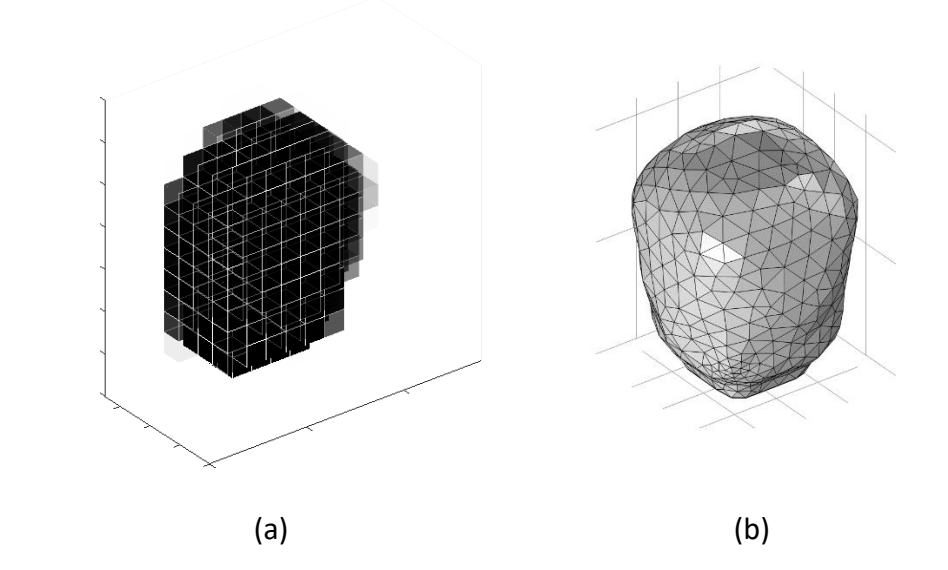


Figure 4 – Resultant optimized topologies for case study #1. (a) Raw topology at iteration 100, and (b) post-processed topology with symmetry conditions recovered.

Figure 4 presents both the optimized and post-processed topologies, and Figure 5 presents their corresponding frequency responses. The volume decreased from 50%, the starting point, to 15.27% at the final iteration, as shown in Figure 4(a), where most of the solid material has been removed from the surroundings of a central solid body. After post-processing, the resultant topology resembles a rounded Balloon-like shape. The FRFs presented in Figure 5 evidence good agreement between the raw and post-processed dynamic responses to harmonic loads, and most importantly, both FRFs evidence an antiresonance at 30 kHz; the design objective has been achieved successfully, therefore demonstrating our design methodology works for the case study.

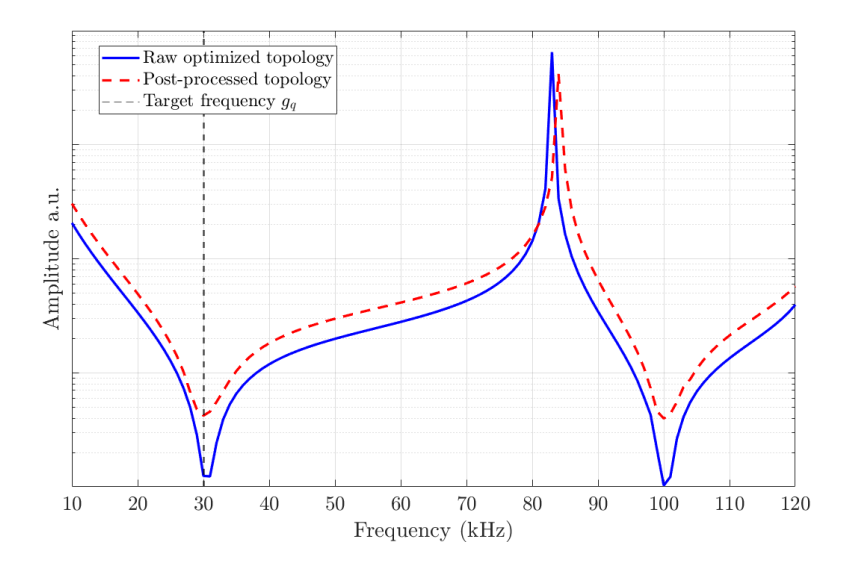


Figure 5 – Frequency response functions for topologies of Figure 4. (a) FRF for the raw optimized topology, and (b) FRF for the post-processed topology.

3.2. Case Study #2.

This case seeks to design a resonator that exhibits an antiresonance at 50 kHz subject to shear (in-plane) harmonic loads, as shown in Figure 2(b). Figure 6 shows the convergence history, Figure 7 shows the optimized topology, and Figure 8 shows the topology's frequency response.

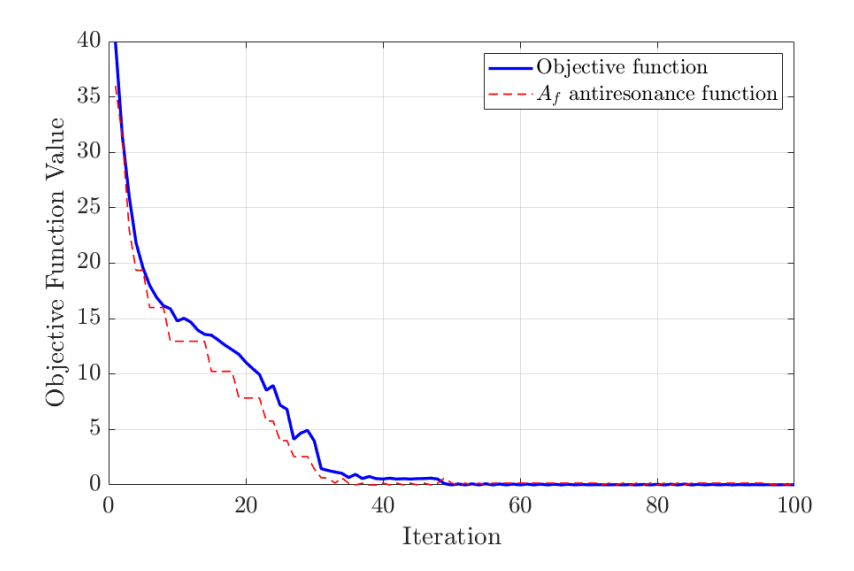


Figure 6 – Convergence history for 100 iterations (solid blue line), and antiresonance function (dashed red line) using A_f from the harmonic-informed routine of Section 2.3.

Figure 6 shows the objective function converging after iteration 50 with a value of 0.01. The antiresonance function, as explained in Section 3.1, was computed to evaluate the correlation between eigenfrequencies and antiresonances. Similar to case study #1, Figure 6 reveals that the eigenfrequencies used to compute the objective function and the identified antiresonances from the FRFs have similar values, validating the harmonic-informed routine effectiveness to select eigenfrequencies by analyzing frequency responses, regardless of different harmonic loads, material properties, dimensions, mesh discretization or target frequency. For this case study, the sudden peaks in the objective function of Figure 3 were not seen. This objective function behavior shows a stable

optimization process where the harmonic-informed selection of eigenmodes routine did not find any other antiresonances in higher frequency ranges during the optimization.

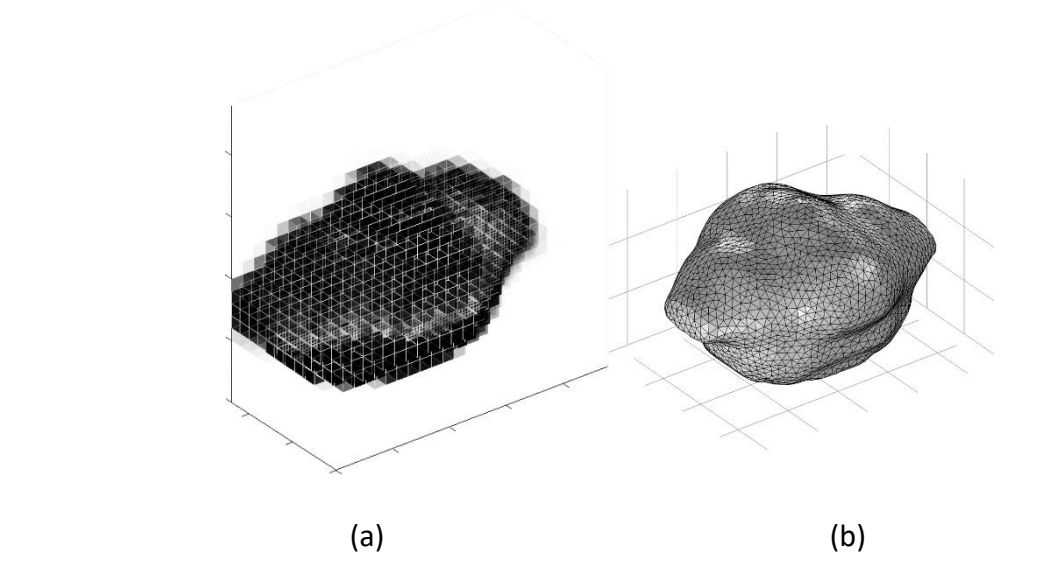


Figure 7 - Resultant optimized topologies for case study #2. (a) Raw topology at iteration 100, and (b) post-processed topology with symmetry conditions recovered.

Figure 7 presents both the optimized and post-processed topologies, and Figure 8 presents their corresponding frequency responses. The volume decreased from 50%, the starting point, to 19.21% at the final iteration, as shown in Figure 7(a), where most of the solid material has been removed from the surroundings of a central solid body. After post-processing, the resultant topology resembles an Asteroid-like shape. Figure 8 presents the FRFs for both topologies, note that the raw topology's FRF was computed from 10 to 150 kHz, while the post-processed topology's FRF was obtained up to 200 kHz to observe the closest resonance peak. In this case study, there are some differences between the raw and post-processed topologies' FRFs. Both topologies have antiresonances around the target frequency, but they do not align as perfectly as in Figure 5. Those differences could be a consequence of using different types of finite elements in a structure subject

mostly to shear stress; the raw topology uses hexahedral elements while the post-processed topology uses tetrahedral elements. Nonetheless, Figure 8 evidence acceptable agreement between the FRFs, both exhibiting an antiresonance around 50 kHz, achieving the design objective and validating our design methodology.

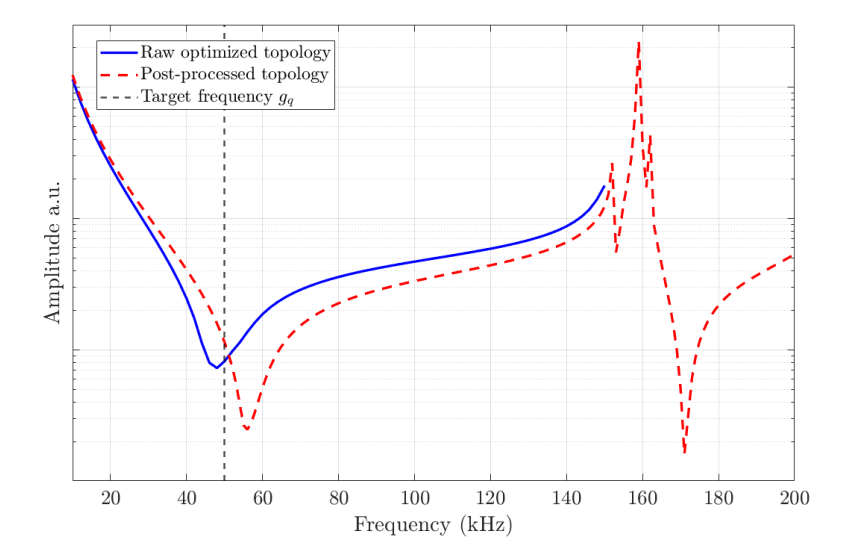


Figure 8 - Frequency response functions for topologies of Figure 7. (a) FRF for the raw optimized topology, and (b) FRF for the post-processed topology.

3.3. Locally Resonant Metasurfaces.

The design methodology proposed in Section 2 can be used to design a structure requiring specific antiresonances; one application is the design of topology-optimized resonators as demonstrated in sections 3.1 and 3.2. These resonators can be arranged to compose ELRM, as it was introduced in Section 1. *Figure* 9 shows a conceptual design of an ELRM composed of 56 topology-optimized resonators from Section 3.1 exemplifying a metasurface that reduce the propagation of surface waves at the resonator's frequency of antiresonance when mounted on top of a surface.

Journal of Mechanical Design

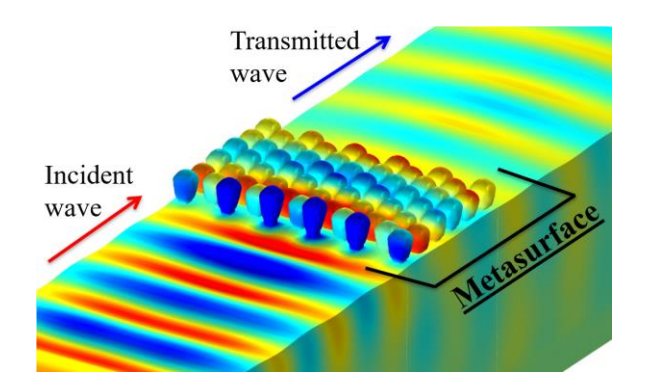


Figure 9 - Total harmonic displacement field of surface waves impinging upon a locally resonant metasurface composed of topology-optimized resonators from Figure 4.

4. CONCLUSIONS

422

423

424

425

426

427

428

429

430

431

432

433

434

435

436

437

438

439

440

441

442

443

A systematic design methodology to realize resonant structures exhibiting antiresonances at desired frequencies subject to specific harmonic loads was proposed as a structural optimization problem using density-based topology optimization. The key advancement to the well-known eigenfrequency matching approach [42] is the new harmonic-informed identification routine that ensures recognition of antiresonance eigenmodes while preventing common problems for this kind of eigenfrequency topology optimization. In other words, the topology optimization problem presented in this paper is fundamentally different from other eigenfrequency matching approaches because it not only matches eigenfrequencies but also analyses frequency responses to select potential eigenmodes to become antiresonances using the identification routine presented in Section 2.3. Even though this approach is computationally more expensive than a simple eigenfrequency matching optimization, it is still faster to compute than a harmonic-based or full dynamic approach, making the design methodology feasible for solving large 3D dynamic problems. Moreover, well-known problems reported in the literature such as localized eigenmodes, repeated eigenfrequencies, or eigenmodes order switching [42], [56], [63] are simple to overcome using the harmonic-informed routine because appropriate eigenmodes are selected for use during the optimization. Additionally, the combination of a density filter with a Heaviside filter contributes to realizing well-defined structures whose dynamic response after post-processing remains coherent to the original optimized topologies. To illustrate these contributions, we have demonstrated how the proposed design methodology provides a robust tool to realize resonant structures for different initial conditions, frequency ranges, material properties, or design domain definitions.

Interesting applications can be developed with the proposed design methodology, for example, an antiresonance at a given frequency is known to generate frequency bandgaps for locally resonant metasurfaces [26]; however, assessing a metasurface performance composed of topology-optimized resonators, such as the ones presented in this paper, is yet to be studied. Beyond the design of acoustic or elastodynamic metasurfaces for wave propagation control at different length scales, the proposed design methodology has broader potential applications, including designing vibration control devices, sensors and actuators, energy harvesting devices, seismic shields, musical instruments, or any other application where the structure's frequency response plays an important role. Moreover, the design methodology has been generalized to accommodate different design objectives, such as matching resonances and antiresonances simultaneously or introducing eigenfrequency gaps for broadband frequency applications.

ACKNOWLEDGMENTS

The authors gratefully acknowledge the support of the National Science Foundation under Grant No. 1934527. Any opinions, findings, conclusions, or recommendations expressed in this material are those of the author(s) and do not necessarily reflect the views of the National Science Foundation. Computations for this research were performed on the Pennsylvania State University's Institute for Computational and Data Sciences' Roar supercomputer.

467 APPENDIX A. 468 Harmonic-informed selection of antiresonance eigenmodes 469 One of the most important components of the design methodology presented in this 470 paper is to appropriately identify and select antiresonance eigenmodes to compute the 471 objective function and sensitivities. Section 2.3 introduced the harmonic-informed 472 selection routine step by step; here, we present a detailed explanation of each step. 473 **Step 1.** Compute antiresonance eigenvalues $\{\lambda\}$ and eigenvectors $[\Phi]$. 474 475 Eigenvalues are required to compute the objective function, eigenvectors are required to 476 identify which eigenmode corresponds to an antiresonance and to compute sensitivities. 477 Note that these eigenmodes must be computed with displacement constraints over the 478 degrees of freedom at which the harmonic load will be applied later to obtain the dynamic 479 response; these are called antiresonance eigenmodes. A generalized eigenproblem 480 provides eigenvalues $\{\lambda\}$ and eigenvectors $[\Phi]$: 481 $[K][\Phi] = {\lambda}[M][\Phi]$ 482 483 **Step 2.** Delete rigid body eigenmodes below a threshold of 1Hz. 484 Once the eigenproblem has been solved, some rigid body modes might appear because 485 the structure is not fully constrained. The simplest way to remove these rigid body modes 486 is thresholding eigenmodes whose eigenfrequency is below 1Hz. 487 Delete eigenmode if $\rightarrow f_A < 1$ Hz 488

- 489 **Step 3.** Remove localized eigenmodes.
- 490 An analysis routine that identifies and removes localized eigenmodes has been
- 491 developed. Since the identified localized eigenmodes are fully removed from the
- 492 optimization, the problem is effectively prevented. This routine removes localized
- 493 eigenmodes following these steps:
- Apply material interpolation models (SIMP or RAMP) and filters to the pseudo-
- density variable ρ from Equations (6) to (9).
- Find solid or near-to-solid elements such that the pseudo-density is higher than
- 497 70%, i.e., $\rho_{\rm hard} = \rho_e > 0.7$. Similarly, find void or near-to-void elements such that
- the pseudo-density is lower than 10%, i.e., $\rho_{\rm soft} = \rho_e > 0.1$.
- \bullet For each eigenvector, extract the displacement at every node for all $ho_{
 m hard}$
- elements; $u_{\rm hard}$, and at every node for all $\rho_{\rm soft}$ elements; $u_{\rm soft}$. Do not consider
- nodes with boundary conditions applied whose displacement is already zero.
- Compute $u_{\text{soft}}/u_{\text{hard}}$ displacement ratios using the following metrics:
- 503 Percentile 90 ratio: PC90($u_{\rm soft}/u_{\rm hard}$)
- 505 Average value ratio: mean(u_{soft})/mean(u_{hard})
- Compute a compound ratio:
- o Ratio_{soft/hard} = (Percentile 90 + Maximum value + Average value)
- Identified localized modes whose compound ratio overpasses a threshold
- criterion establish as Threshold = 1×10^3 , such that:
- 510 \circ Localized mode identified if \rightarrow Ratio_{soft/solid} > Threshold

511

- 512 **Step 4.** Compute the topology's frequency response subject to harmonic loads.
- The displacement constraints used to compute the antiresonance eigenmodes must be replaced by the harmonic loads to evaluate how antiresonances happen in the frequency domain. The frequency responses at the nodes of interest are obtained by solving the
- generalized dynamic problem subject to harmonic loads:

517
$$[M]\{\ddot{x}\} + [C]\{\dot{x}\} + [K]\{x\} = \{F_{\text{Harmonic}}\}$$

- 519 **Step 5.** Analyze harmonic responses and identify an antiresonance frequency.
- 520 To properly identify antiresonances, the FRFs must be analyzed using the following steps:
- Extract the FRFs on each of the nodes where the harmonic load has been applied.
- Compute the average FRF over all the aforementioned nodes:
- 523 o averaged FRF = mean(FRF)
- Find local antiresonance peaks using the MATLAB function findpeaks:
- 525 [Amplitude,idx,Width,Prominence] = findpeaks(1/averaged FRF)
- Evaluate local peak frequency absolute distance to target frequency g_a :
- 527 Proximity = abs(Target frequency Peak Frequency)
- Evaluate metrics for each local antiresonance peak identified, i.e., antiresonance
- bandwidth, amplitude, prominence, and proximity to the target frequency g_q . Use
- 530 the combined antiresonance evaluation factor:
- o factor = Amplitude + Prominence + Width Proximity

532	Select the local antiresonance peak with the highest evaluation factor as the
533	identified antiresonance frequency A_f .
534	Note the following metric definitions [64]:
535	Amplitude: signal value of a data sample that is either larger than its two
536	neighboring samples or is equal to infinite.
537	Prominence: measures how much the peak stands out due to its intrinsic height
538	and its location relative to other peaks.
539	Width: distance between the points where the signal intercepts a horizontal
540	reference line positioned beneath the peak at a vertical distance equal to half the
541	peak prominence.
542	• Proximity: measures the distance in Hertz (Hz) from the target frequency to the
543	identified antiresonance frequency peak.
544	
545	Step 5. Select an antiresonance eigenfrequency mode.
546	Once an antiresonance frequency ${\cal A}_f$ is identified, the corresponding topology's harmonic
547	displacement response is matched with an antiresonance mode shape (eigenvector) using
548	the Modal Assurance Criterion (MAC) [48]. The following steps are used to identify an
549	appropriate eigenmode:
550	$ullet$ Extract the harmonic displacement response $oldsymbol{x}_H$ at the identified frequency A_f .
551	$ullet$ Compute the MAC between the harmonic displacement response $oldsymbol{x}_H$ and every
552	antiresonance eigenvector $oldsymbol{\Phi}_{A}$:

Journal of Mechanical Design

553	$MAC = \frac{ \boldsymbol{\phi}_A^T \boldsymbol{x}_H ^2}{(\boldsymbol{\phi}_A^T \boldsymbol{\phi}_A)(\boldsymbol{\phi}_A^T \boldsymbol{x}_H)}$
554	• Select the eigenmode with the highest MAC coefficient as the identified
555	antiresonance eigenmode; its corresponding eigenvalue $\lambda_A = \left(2\pi f_q ight)^2$ is to be
556	used during the optimization in Equation (1) .
557	

558 APPENDIX B.

Impact of penalization factors on localized eigenmodes

Non-zero finite frequencies localized in the void or near-to-void regions are not preventable just by setting the stiffness and mass penalization factors to different values, e.g. $p_K=3$, $p_M=1$, or by modifying the stiffness-to-mass penalization ratio p_K/p_M in low-density regions. This problem is neither fully preventable by setting both penalization factors to the same value as we did in the case studies in Section 3, i.e. $p_K=p_M=1$, however, the number of localized modes is greatly reduced while the computation time is improved using equal penalization factors. To illustrate this statement, consider a simple demonstration. Figure Appendix B.1 shows a design domain manually created, containing a solid non-design stem surrounded by low-density elements. The stem comprises 2% of the available solid space; the remaining 98% of space has near-to-void density elements, a perfect scenario to observe localized modes in low-density regions.

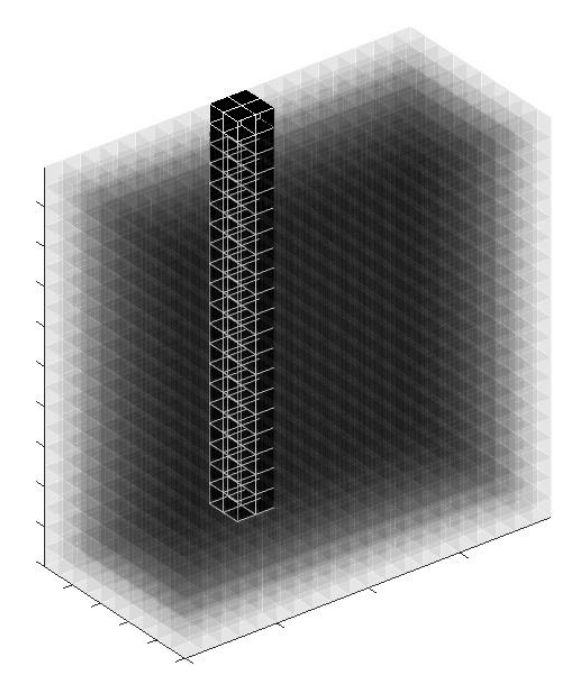


Figure Appendix B.1. Design domain with homogeneous low-density material surrounding a solid stem.

The eigenproblem is solved using both the SIMP and the RAMP models, Equations (6) and (7), with both the same and different penalization factors for the stiffness (p_K) and mass (p_M) matrices. In the frequency range between 10kHz and 50kHz, the stem has three eigenmodes: two flexural modes and one extensional mode. Table Appendix B.1 shows all the eigenfrequencies obtained with the SIMP model. Table Appendix B.2 shows all the eigenfrequencies obtained with the RAMP model. We have used the localized eigenmode recognition routine from APPENDIX A. to differentiate localized modes from real modes. Note that in the following tables, the localized eigenmodes are in red while the real modes are in black boldface. Finally, Table Appendix B.3 shows the computation time required to solve each eigenproblem.

Table Appendix B.1. Eigenfrequencies obtained using SIMP model (Hz).

$p_K = 1$	$p_K = 3$			$p_K = 3$		
$p_M=1$	$p_{M} = 3$			$p_M=1$		
18511	17876	12511	15524	17787	18983	19947
19099	19153	12537	15629	17963	19000	19988
23272	21770	12710	15650	17984	19018	20055
24233	22670	12756	15709	18093	19035	20061
26876	25644	13070	15902	18123	19069	20155
35773	35104	13154	15942	18130	19231	20454
36377	35369	13488	16525	18240	19295	20488
37952	37443	14004	16633	18254	19301	20578
40050	38567	14418	16731	18293	19354	20587
40636	39061	14588	16847	18429	19364	20608
43469	42500	14595	16896	18551	19368	20670
44489	43492	14611	17087	18569	19502	20816
45850	45199	14620	17308	18609	19529	20925
46572	46117	15128	17567	18635	19547	21056
48305	47864	15188	17613	18685	19662	21059
	49712	15469	17631	18885	19663	21145

Table Appendix B.2. Eigenfrequencies obtained using RAMP model (Hz).

$p_K = 1$	$p_{K} = 3$	$p_{K} = 3$	
$p_{M} = 1$	$p_M = 3$	p_{M}	= 1
18679	18203	16455	36994
18791	19048	17131	37906
23271	23271	17159	38805
24232	24232	18100	39216
26875	26875	19004	40077
35774	35774	25296	42393
36377	36377	25722	42557
37952	37952	26836	43743
39967	39156	28320	44560
40050	40050	30738	44836
43469	43469	31459	45650
44489	44489	32421	46911
45850	45850	32932	47159
46572	46572	34157	47828
48305	48305	35985	49636
		36755	

Table Appendix B.3. SIMP vs RAMP model computation time in seconds (s).

SIMP model			
$p_K = 1$ $p_M = 1$	$p_K = 3$ $p_M = 3$	$p_K = 3$ $p_M = 1$	
68 (s)	71 (s)	523 (s)	

RAMP model			
$p_K = 1$ $p_M = 1$	$p_K = 3$ $p_M = 3$	$p_K = 3$ $p_M = 1$	
70 (s)	69 (s)	90 (s)	

These results demonstrate that using different penalization factors not only leads to significantly more localized modes but also to higher computation time, especially when the SIMP model is used. It also shows that when using the same penalization factors, fewer localized modes are obtained while improving computation time.

596 APPENDIX C.

Volume constraints study

Section 3 presented topologies where volume constraints are not active during the optimization process as they are not needed to converge to optimized solutions; the design objective is achieved regardless of volume constraints. Here, we present a comparative study on how different volume constraints influence the solution.

Consider the following demonstration to illustrate the volume constraint effect. For the same design problem of Section 3.1 a set of optimized topologies are obtained by varying the maximum volume constraint while keeping all the optimization parameters from Table 1 the same. The selected maximum volume constraints are 100%, 90%, 80%, 70%, 60%, 50%, 40%, 30%, and 20%. Figure Appendix C.1. presents the volume evolution as a function of the iteration number for each of the maximum volume constraints considered. The starting point is always the maximum volume fraction for all design variables, except for the bottom layer of elements, as explained in Section 3. Please note that the 10% volume constraint case was also considered, but this low percentage results in an overconstrained problem for which no feasible solution is found.

Note that in all the cases presented in Figure Appendix C.1., the imposed volume constraint is never active, i.e., the optimization never attempts to push the volume to the constraint. Instead, the volume fraction is freely reduced by the optimization, converging to a certain volume fraction after 100 iterations. For the cases with the maximum volume

constraint of 40%, 30%, and 20%, the convergence occurs around 17%. When the constraint is set to 50%, the convergence value is around a volume fraction of 27%. The convergence points for the other cases are not shown as they are not reached after 100 iterations. The convergence point is different because of disconnected members adding to the volume without decreasing the design objective; if the disconnected members are excluded, the converge point would be similar irrespective of the initially set volume constraint. This analysis indicates that the volume constraints are never active during the optimization process as they neither improve nor deteriorate the optimization results.

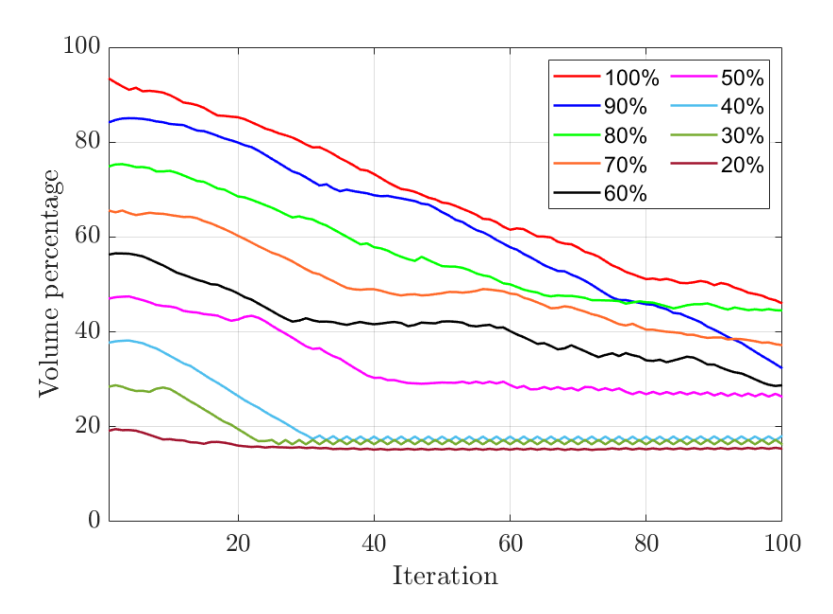
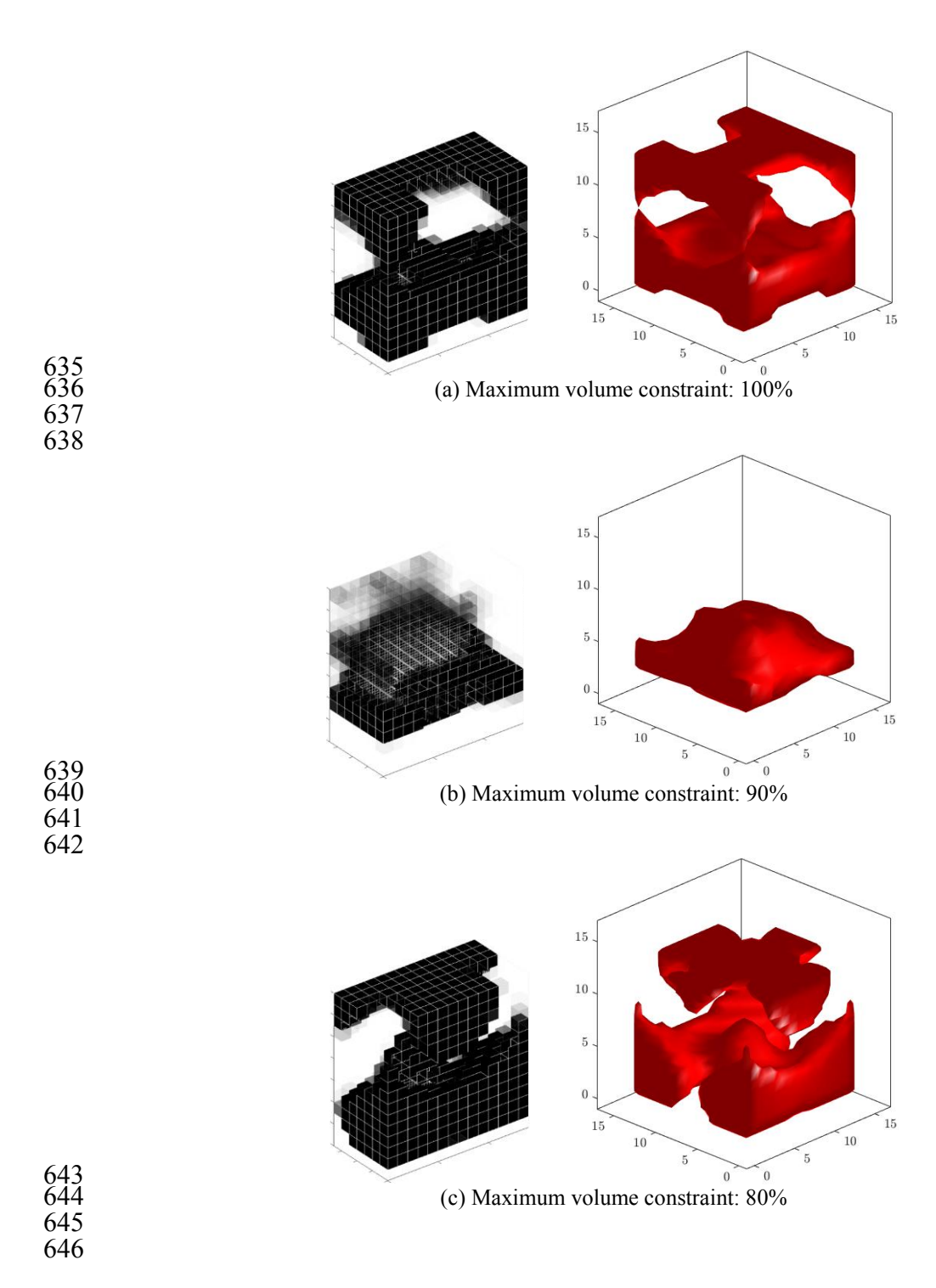
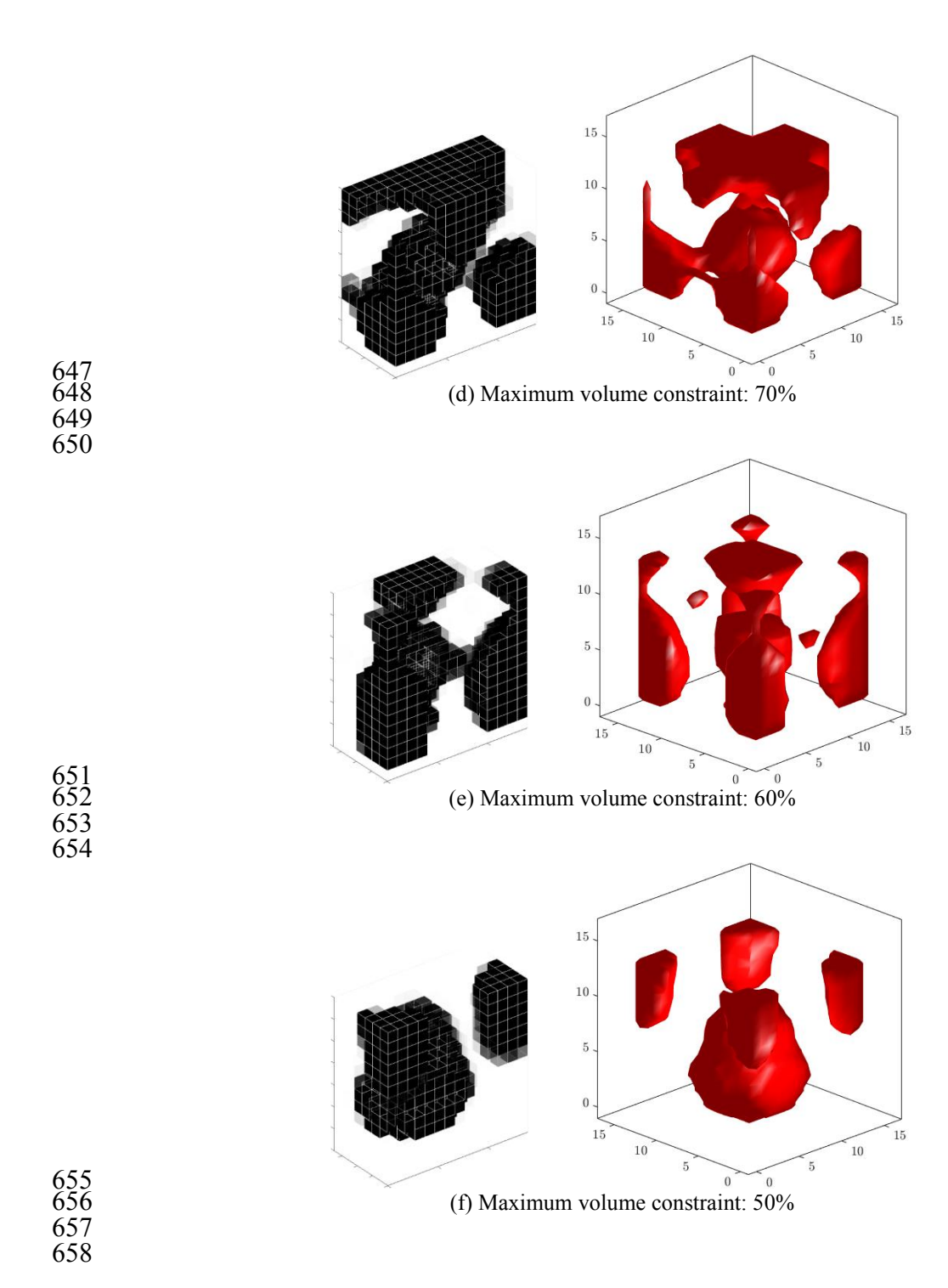


Figure Appendix C.1. Volume evolution using different maximum volume constraints.

Figure Appendix C.2 shows the topologies obtained at iteration 100 for each maximum volume constraint considered. Each subfigure shows the raw topology on the left-hand side and the binarized topology on the right-hand side. Note that the raw topologies show half of the structure as it includes a symmetry condition, while the binarized topologies present a post-processed topology with its symmetry recovered.





671

672

673

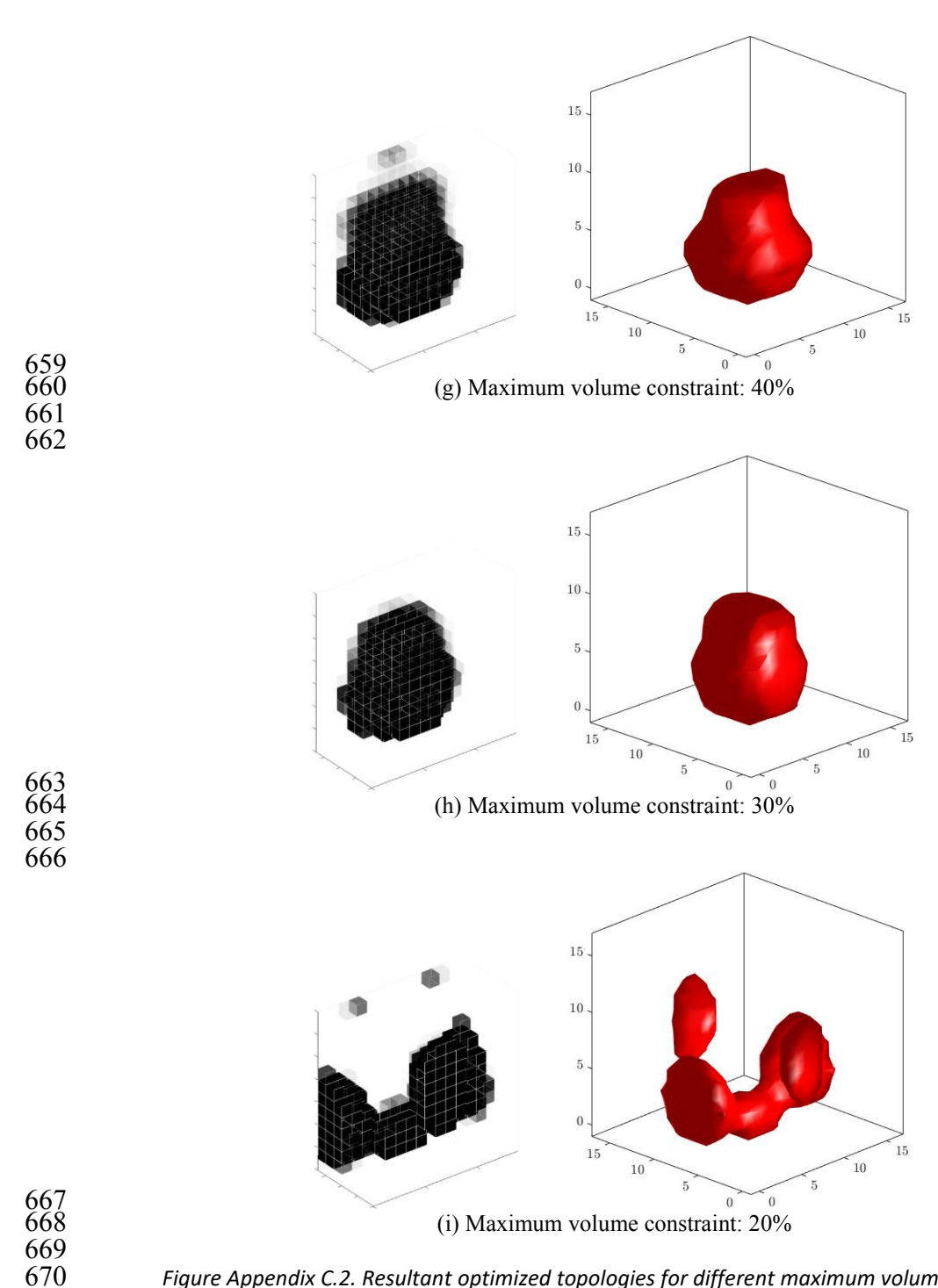


Figure Appendix C.2. Resultant optimized topologies for different maximum volume constraints.

The resultant topologies in Figure Appendix C.2 show that a volume constraint does not prevent disconnected members and that well-defined topologies are achieved regardless of the constraint value. Interestingly, when using the volume constraint of 90% the resultant topology does not exhibit disconnected members. When the volume constraint is set to a lower value, the amount of available material is reduced, therefore the optimization removes unnecessary material as seen for the cases of 40% and 30%; however, when the volume constraint is further reduced, the optimization finds solutions in a more constrained solution space, leading to different topologies and disconnected members, as shown in the case of volume constraint 20%. If the volume constraint is set to even lower values, i.e., 10% or 15%, the optimization becomes over-constrained and does not find feasible solutions. This observation suggests that disconnected members can be obtained with both high and low volume constraint values. Therefore, finding an appropriate constraint value requires a search that must be attempted heuristically for every design problem.

Disconnected members do not influence the solution as they do not contribute to the design objective. Consider the optimized topology shown in Figure Appendix C.3. The disconnected elements have been manually removed from the raw topology and both frequency responses, with and without disconnected elements, have been computed. Please note that the typical post-processing does not remove these disconnected elements directly from the raw topology. Instead, the raw topology is binarized to obtain fully solid members with properly defined boundaries, then, disconnected parts can be discarded before meshing and simulating the final post-processed topology.

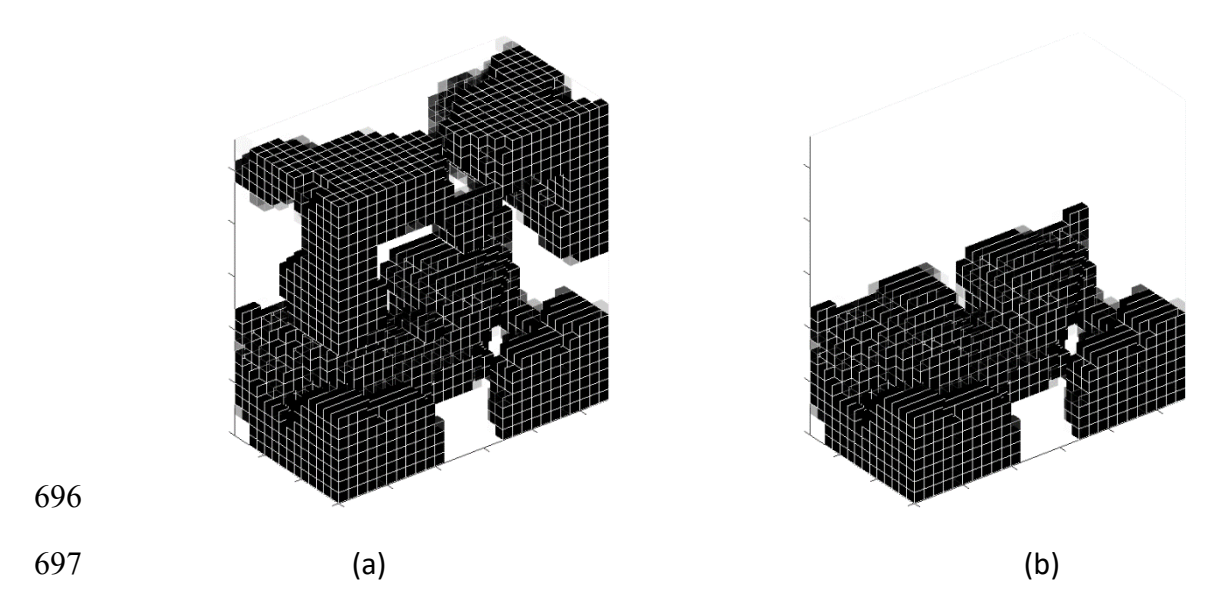


Figure Appendix C.3. Optimized topology with disconnected members. (a) original raw topology, and (b) raw topology with disconnected elements manually removed.

objective while maintaining high-quality metrics in their dynamic responses, as shown and

Figure Appendix C.4 compares the frequency responses for the original topology and the manually-removed elements topology, demonstrating that both frequency responses are the same. Any differences come from post-processing steps because small deviations from the raw topology might result in frequency response changes. This is especially critical for very small structural features that after post-processing could change significantly. Despite some differences, the original and the post-processed topologies achieved the design

discussed throughout the results section.

709

707

708

698

699

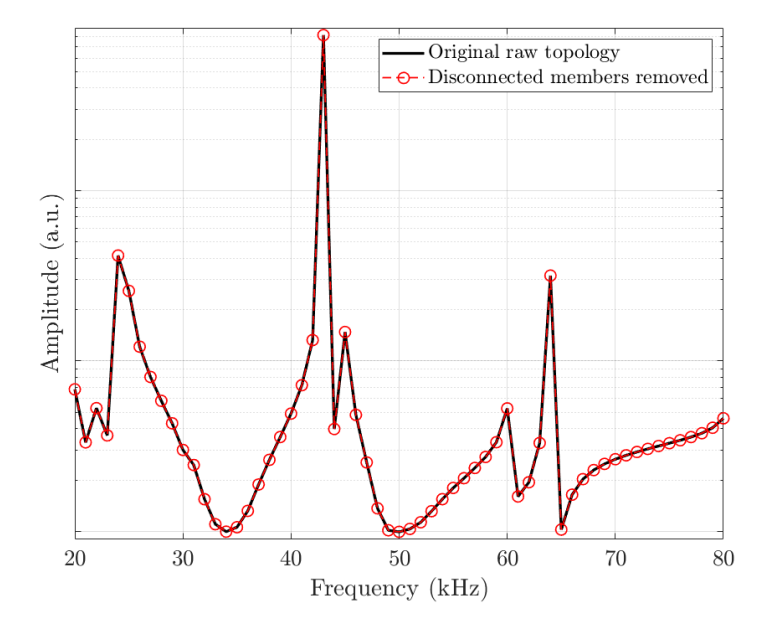


Figure Appendix C.4. Frequency response functions for topologies presented in Figure Appendix C.3.

Differences between the raw and post-processed frequency response can be minimized by adjusting the threshold value used during the binarization process. This threshold controls how the boundaries are defined; a higher threshold reduces the amount of solid material; a lower threshold increases solid material. In the proposed design methodology, the threshold value is always set to 50% because this value does not promote solid material over void space, and vice versa. All the presented results were post-processed using the same threshold value to maintain consistency; therefore, frequency response differences are expected.

REFERENCES

- 723 [1] Z. Liu *et al.*, "Locally resonant sonic materials," *Science (80-.).*, vol. 289, no. 5485, pp. 1734—1736, Sep. 2000, doi: 10.1126/SCIENCE.289.5485.1734/ASSET/CC705932-9BCD-42ED-A907-5221FAFE302A/ASSETS/GRAPHIC/SE3308780004.JPEG.
- 727 [2] T. Lee and H. Iizuka, "Bragg scattering based acoustic topological transition 728 controlled by local resonance," *Phys. Rev. B*, vol. 99, no. 6, p. 064305, Feb. 2019, 729 doi: 10.1103/PHYSREVB.99.064305/FIGURES/8/MEDIUM.
- 730 [3] F. Lemoult, N. Kaina, M. Fink, and G. Lerosey, "Wave propagation control at the deep subwavelength scale in metamaterials," *Nat. Phys.*, vol. 9, no. 1, pp. 55–60, 2013, doi: 10.1038/nphys2480.
- 733 [4] F. Zeighami, A. Palermo, and A. Marzani, "Rayleigh waves in locally resonant metamaterials," *Int. J. Mech. Sci.*, vol. 195, no. December 2020, 2021, doi: 10.1016/j.ijmecsci.2020.106250.
- 736 [5] A. Palermo and A. Marzani, "Control of Love waves by resonant metasurfaces," *Sci. Rep.*, vol. 8, no. 1, pp. 1–8, 2018, doi: 10.1038/s41598-018-25503-8.
- 738 [6] A. Colombi, P. Roux, S. Guenneau, P. Guéguen, and R. V. Craster, "Forests as a natural seismic metamaterial: Rayleigh wave bandgaps induced by local resonances," *Sci. Rep.*, vol. 6, no. January, pp. 1–7, 2016, doi: 10.1038/srep19238.
- 741 [7] A. Colombi, D. Colquitt, P. Roux, S. Guenneau, and R. V. Craster, "A seismic metamaterial: The resonant metawedge," *Sci. Rep.*, vol. 6, no. Umr 7249, pp. 1–6, 2016, doi: 10.1038/srep27717.
- 744 [8] D. Colquitt, A. Colombi, R. V. Craster, P. Roux, and S. Guenneau, "Seismic metasurfaces: Sub-wavelength resonators and Rayleigh wave interaction," *J. Mech. Phys. Solids*, vol. 99, no. November 2016, pp. 379–393, 2017, doi: 10.1016/j.jmps.2016.12.004.
- 748 [9] Y.-C. Su and C.-K. Wu, "A snowman-like seismic metamaterial," *J. Appl. Phys.*, vol. 132, no. 10, p. 105106, Sep. 2022, doi: 10.1063/5.0098429.
- 750 [10] M. Rupin, F. Lemoult, G. Lerosey, and P. Roux, "Experimental demonstration of ordered and disordered multiresonant metamaterials for lamb waves," *Phys. Rev. Lett.*, vol. 112, no. 23, pp. 1–5, 2014, doi: 10.1103/PhysRevLett.112.234301.
- 753 [11] R. Zaccherini *et al.*, "Locally Resonant Metasurfaces for Shear Waves in Granular 754 Media," *Phys. Rev. Appl.*, vol. 13, no. 3, p. 1, 2020, doi: 755 10.1103/PhysRevApplied.13.034055.
- 756 [12] M. Lott, P. Roux, S. Garambois, P. Guéguen, and A. Colombi, "Evidence of metamaterial physics at the geophysics scale: The METAFORET experiment," 758 Geophys. J. Int., vol. 220, no. 2, pp. 1330–1339, 2020, doi: 10.1093/gji/ggz528.
- 759 [13] C. Boutin, L. Schwan, and M. S. Dietz, "Elastodynamic metasurface: Depolarization of mechanical waves and time effects," *J. Appl. Phys.*, vol. 117, no. 6, p. 064902, 761 Feb. 2015, doi: 10.1063/1.4908135.
- 762 [14] S. Brûlé, E. H. Javelaud, S. Enoch, and S. Guenneau, "Experiments on seismic metamaterials: Molding surface waves," *Phys. Rev. Lett.*, vol. 112, no. 13, pp. 1–5, 2014, doi: 10.1103/PhysRevLett.112.133901.

- 765 [15] Z. Liu, S. B. Shan, H. W. Dong, and L. Cheng, "Topologically customized and
 766 surface-mounted meta-devices for Lamb wave manipulation," Smart Mater.
 767 Struct., vol. 31, no. 6, 2022, doi: 10.1088/1361-665X/ac64db.
- 768 [16] W. Jiang, Y. Zhu, G. Yin, H. Lu, L. Xie, and M. Yin, "Dispersion relation prediction 769 and structure inverse design of elastic metamaterials via deep learning," *Mater.* 770 *Today Phys.*, vol. 22, p. 100616, Jan. 2022, doi: 10.1016/J.MTPHYS.2022.100616.
- 771 [17] S. Halkjær, O. Sigmund, and J. S. Jensen, "Maximizing band gaps in plate structures," *Struct. Multidiscip. Optim.*, vol. 32, no. 4, pp. 263–275, 2006, doi: 10.1007/s00158-006-0037-7.
- 774 [18] J. H. Oh, Y. K. Ahn, and Y. Y. Kim, "Maximization of operating frequency ranges of hyperbolic elastic metamaterials by topology optimization," *Struct. Multidiscip.* 776 Optim., vol. 52, no. 6, pp. 1023–1040, 2015, doi: 10.1007/s00158-015-1288-y.
- 777 [19] J. Zhang, Y. Li, T. Zhao, Q. Zhang, L. Zuo, and K. Zhang, "Machine-learning based design of digital materials for elastic wave control," *Extrem. Mech. Lett.*, vol. 48, p. 101372, Oct. 2021, doi: 10.1016/J.EML.2021.101372.
- 780 [20] O. Sigmund and J. Sø. Jensen, "Systematic design of phononic band-gap materials and structures by topology optimization," in *Philosophical Transactions of the Royal Society A: Mathematical, Physical and Engineering Sciences*, 2003, vol. 361, no. 1806, pp. 1001–1019, doi: 10.1098/rsta.2003.1177.
- Z. Wang, W. Xian, M. R. Baccouche, H. Lanzerath, Y. Li, and H. Xu, "Design of Phononic Bandgap Metamaterials Based on Gaussian Mixture Beta Variational Autoencoder and Iterative Model Updating," J. Mech. Des., vol. 144, no. 4, Apr. 2022, doi: 10.1115/1.4053814.
- 788 [22] H. W. Dong, S. D. Zhao, Y. S. Wang, and C. Zhang, "Topology optimization of anisotropic broadband double-negative elastic metamaterials," *J. Mech. Phys. Solids*, vol. 105, pp. 54–80, 2017, doi: 10.1016/j.jmps.2017.04.009.
- 791 [23] X. Yang and Y. Y. Kim, "Topology optimization for the design of perfect mode-792 converting anisotropic elastic metamaterials," *Compos. Struct.*, vol. 201, no. April, 793 pp. 161–177, 2018, doi: 10.1016/j.compstruct.2018.06.022.
- 794 [24] B. Ahn, H. Lee, J. S. Lee, and Y. Y. Kim, "Topology optimization of metasurfaces for anomalous reflection of longitudinal elastic waves," *Comput. Methods Appl.* 796 *Mech. Eng.*, vol. 357, p. 112582, 2019, doi: 10.1016/j.cma.2019.112582.
- 797 [25] R. T. Wu, T. W. Liu, M. R. Jahanshahi, and F. Semperlotti, "Design of one-dimensional acoustic metamaterials using machine learning and cell concatenation," *Struct. Multidiscip. Optim.*, vol. 63, no. 5, pp. 2399–2423, May 2021, doi: 10.1007/S00158-020-02819-6/TABLES/18.
- 801 [26] C. J. Lissenden, C. N. Hakoda, and P. Shokouhi, "Control of low-frequency Lamb wave propagation in plates by boundary condition manipulation," *J. Appl. Phys.*, vol. 129, no. 9, 2021, doi: 10.1063/5.0042576.
- L. S. S. Pillarisetti, C. J. Lissenden, and P. Shokouhi, "Understanding the role of resonances and anti-resonances in shaping surface-wave bandgaps for metasurfaces," *J. Appl. Phys.*, vol. 132, no. 16, p. 164901, Oct. 2022, doi: 10.1063/5.0093083.
- 808 [28] D. G. Guzman, L. S. S. Pillarisetti, S. Sridhar, C. J. Lissenden, M. Frecker, and P.

- Shokouhi, "Design of resonant elastodynamic metasurfaces to control SO Lamb waves using topology optimization," *JASA Express Lett.*, vol. 2, no. 11, p. 115601, Nov. 2022, doi: 10.1121/10.0015123.
- 812 [29] M. P. Bendsøe, A. Díaz, and N. Kikuchi, "Topology and Generalized Layout
 813 Optimization of Elastic Structures," *Topol. Des. Struct.*, pp. 159–205, 1993, doi: 10.1007/978-94-011-1804-0 13.
- 815 [30] O. Sigmund and M. P. Bendsøe, "Topology optimization: from airplanes to nanooptics," *Bridg. from Technol. to Soc.*, pp. 40–51, 2004.
- 817 [31] O. Sigmund and K. Maute, "Topology optimization approaches: A comparative review," *Struct. Multidiscip. Optim.*, vol. 48, no. 6, pp. 1031–1055, 2013, doi: 10.1007/s00158-013-0978-6.
- 820 [32] N. P. Van Dijk, K. Maute, M. Langelaar, and F. Van Keulen, "Level-set methods for structural topology optimization: A review," *Struct. Multidiscip. Optim.*, vol. 48, no. 3, pp. 437–472, 2013, doi: 10.1007/s00158-013-0912-y.
- S. Zargham, T. A. Ward, R. Ramli, and I. Anjum Badruddin, "Topology optimization: a review for structural designs under vibration problems," *Struct. Multidiscip. Optim.*, vol. 53, pp. 1157–1177, 2016, doi: 10.1007/s00158-015-1370-5.
- X. Zhang, Z. Kang, and W. Zhang, "Robust topology optimization for dynamic compliance minimization under uncertain harmonic excitations with inhomogeneous eigenvalue analysis," *Struct. Multidiscip. Optim.*, vol. 54, no. 6, pp. 1469–1484, Dec. 2016, doi: 10.1007/S00158-016-1607-Y/TABLES/4.
- 831 [35] O. M. Silva, M. M. Neves, and A. Lenzi, "On the use of active and reactive input power in topology optimization of one-material structures considering steady-state forced vibration problems," *J. Sound Vib.*, vol. 464, p. 114989, Jan. 2020, doi: 10.1016/J.JSV.2019.114989.
- [36] O. M. Silva, M. M. Neves, and A. Lenzi, "A critical analysis of using the dynamic compliance as objective function in topology optimization of one-material structures considering steady-state forced vibration problems," *J. Sound Vib.*, vol. 444, pp. 1–20, Mar. 2019, doi: 10.1016/J.JSV.2018.12.030.
- J. S. Jensen, "Topology optimization of dynamics problems with Padé
 approximants," *Int. J. Numer. Methods Eng.*, vol. 72, no. 13, pp. 1605–1630, 2007,
 doi: 10.1002/nme.2065.
- 842 [38] Q. Li, O. Sigmund, J. S. Jensen, and N. Aage, "Reduced-order methods for dynamic problems in topology optimization: A comparative study," *Comput. Methods Appl. Mech. Eng.*, vol. 387, p. 114149, Dec. 2021, doi: 10.1016/J.CMA.2021.114149.
- 845 [39] N. Olhoff and J. Du, "Generalized incremental frequency method for topological designof continuum structures for minimum dynamic compliance subject to forced vibration at a prescribed low or high value of the excitation frequency," Struct. Multidiscip. Optim., vol. 54, no. 5, pp. 1113–1141, Nov. 2016, doi: 10.1007/S00158-016-1574-3/TABLES/7.
- 850 [40] N. L. Pedersen, "Maximization of eigenvalues using topology optimization," 851 Struct. Multidiscip. Optim., vol. 20, no. 1, pp. 2–11, 2000, doi: 852 10.1007/s001580050130.

- J. S. Jensen and N. L. Pedersen, "On maximal eigenfrequency separation in two-material structures: The 1D and 2D scalar cases," *J. Sound Vib.*, vol. 289, no. 4–5, pp. 967–986, 2006, doi: 10.1016/j.jsv.2005.03.028.
- Z.-D. Ma, H.-C. Cheng, and N. Kikuchi, "Structural Design for Obtaining Desired
 Eigenfrequencies by using the Topology and Shape Optimization Method,"
 Comput. Syst. Eng., vol. 5, no. 1, pp. 77–89, 1994.
- 859 [43] W. B. Jeong, W. S. Yoo, and J. Y. Kim, "Sensitivity analysis of anti-resonance 860 frequency for vibration test control of a fixture," *KSME Int. J.*, vol. 17, no. 11, pp. 861 1732–1738, 2003, doi: 10.1007/BF02983603.
- M. Geradin and D. J. Rixen, "Mechanical Vibrations: Theory and Application to
 Structural Dynamics 3rd Edition M. Geradin and D. J. Rixen John Wiley and Sons,
 The Atrium, Southern Gate, Chichester, West Sussex, PO19 8SQ, UK. 2015. 598pp.
 Illustrated. £83.95. ISBN 978-1-118-90020 8.," *Aeronaut. J.*, vol. 122, no. 1251, pp.
 857–857, May 2018, doi: 10.1017/AER.2018.27.
- S. Rojas-Labanda and M. Stolpe, "Benchmarking optimization solvers for structural topology optimization," *Struct. Multidiscip. Optim.*, vol. 52, no. 3, pp. 527–547, 2015, doi: 10.1007/s00158-015-1250-z.
- 870 [46] R. T. Haftka and Z. Gürdal, *Elements of Structural Optimization*, vol. 11. Dordrecht: Springer Netherlands, 1992.
- [47] L. Lamberti and C. Pappalettere, "Move limits definition in structural optimization with sequential linear programming. Part I: Optimization algorithm," *Comput. Struct.*, vol. 81, no. 4, pp. 197–213, May 2003, doi: 10.1016/S0045-7949(02)00442-X.
- 876 [48] M. Pastor, M. Binda, and T. Harčarik, "Modal Assurance Criterion," *Procedia Eng.*, vol. 48, pp. 543–548, Jan. 2012, doi: 10.1016/J.PROENG.2012.09.551.
- 878 [49] M. P. Bendsøe and O. Sigmund, "Material interpolation schemes in topology optimization," *Arch. Appl. Mech.*, vol. 69, no. 9–10, pp. 635–654, 1999, doi: 10.1007/s004190050248.
- 881 [50] M. P. Bendsøe, "Optimal shape design as a material distribution problem," *Struct. Optim.*, vol. 1, no. 4, pp. 193–202, 1989, doi: 10.1007/BF01650949.
- 883 [51] M. Stolpe and K. Svanberg, "An alternative interpolation scheme for minimum compliance topology optimization," *Struct. Multidiscip. Optim.*, vol. 22, no. 2, pp. 116–124, 2001, doi: 10.1007/s001580100129.
- J. Du and N. Olhoff, "Topological design of freely vibrating continuum structures for maximum values of simple and multiple eigenfrequencies and frequency gaps," *Struct. Multidiscip. Optim.*, vol. 34, no. 2, pp. 91–110, 2007, doi: 10.1007/s00158-007-0101-y.
- 890 [53] D. Tcherniak, "Topology optimization of resonating structures using SIMP method," *Int. J. Numer. Methods Eng.*, vol. 54, no. 11, pp. 1605–1622, 2002, doi: 10.1002/nme.484.
- 893 [54] M. Bruyneel and P. Duysinx, "Note on topology optimization of continuum 894 structures including self-weight," *Struct. Multidiscip. Optim.*, vol. 29, no. 4, pp. 895 245–256, Apr. 2005, doi: 10.1007/s00158-004-0484-y.
- 896 [55] Z. Qiao, Z. Weihong, Z. Jihong, and G. Tong, "Layout optimization of multi-

- component structures under static loads and random excitations," *Eng. Struct.*, vol. 43, pp. 120–128, Oct. 2012, doi: 10.1016/J.ENGSTRUCT.2012.05.013.
- Z. Li, T. Shi, and Q. Xia, "Eliminate localized eigenmodes in level set based topology optimization for the maximization of the first eigenfrequency of vibration," *Adv. Eng. Softw.*, vol. 107, pp. 59–70, 2017, doi: 10.1016/j.advengsoft.2016.12.001.
- 903 [57] T. S. Kim and Y. Y. Kim, "MAC-based mode-tracking in structural topology optimization," *Comput. Struct.*, vol. 74, no. 3, pp. 375–383, 2000, doi: 10.1016/S0045-7949(99)00056-5.
- 906 [58] M. M. Neves, H. Rodrigues, and J. M. Guedes, "Generalized topology design of structures with a buckling load criterion," *Struct. Optim.*, vol. 10, no. 2, pp. 71–78, Oct. 1995, doi: 10.1007/BF01743533/METRICS.
- J. H. Rong, Z. L. Tang, Y. M. Xie, and F. Y. Li, "Topological optimization design of
 structures under random excitations using SQP method," *Eng. Struct.*, vol. 56, pp.
 2098–2106, 2013, doi: 10.1016/j.engstruct.2013.08.012.
- 912 [60] X. Zhang and Z. Kang, "Vibration suppression using integrated topology 913 optimization of host structures and damping layers," *JVC/Journal Vib. Control*, vol. 914 22, no. 1, pp. 60–76, 2016, doi: 10.1177/1077546314528368.
- 915 [61] S. Xu, Y. Cai, and G. Cheng, "Volume preserving nonlinear density filter based on heaviside functions," *Struct. Multidiscip. Optim.*, vol. 41, no. 4, pp. 495–505, 2010, doi: 10.1007/s00158-009-0452-7.
- 918 [62] G. Papazafeiropoulos, M. Muñiz-Calvente, and E. Martínez-Pañeda,
 919 "Abaqus2Matlab: A suitable tool for finite element post-processing," *Adv. Eng.* 920 Softw., vol. 105, pp. 9–16, Mar. 2017, doi: 10.1016/J.ADVENGSOFT.2017.01.006.
- [63] Y. Maeda, S. Nishiwaki, K. Izui, M. Yoshimura, K. Matsui, and K. Terada,
 "Structural topology optimization of vibrating structures with specified
 eigenfrequencies and eigenmode shapes," *Int. J. Numer. Methods Eng.*, vol. 67,
 no. 5, pp. 597–628, 2006, doi: 10.1002/nme.1626.
- 925 [64] T. M. Inc., "Signal Processing Toolbox (R2022b)." The MathWorks Inc., 2022, 926 [Online]. Available: https://www.mathworks.com/help/signal/ref/findpeaks.html. 927